Clay Minerals (2026), **61**, 271–276
doi:10.1180/clm.2026.10052

CAMBRIDGE UNIVERSITY PRESS

Article

Hydrogen adsorption properties of Ag-exchanged clinoptilolite

Burcu Erdoğan and Orkun Ergürhan
Department of Physics, Eskişehir Technical University Faculty of Science: Eskisehir Teknik Universitesi, Türkiye

Abstract

Our energy needs must be met by envssironmentally friendly energy sources such as hydrogen energy because fossil fuels are being depleted and are restricted by CO_2 emissions. One way to safely store hydrogen is to use porous materials, such as clinoptilolite (CLN), for physical adsorption. In this study, the effect of cation exchange with Ag^+ on the hydrogen adsorption properties of Gördes CLN was investigated. The Ag-modified forms were obtained by treating the CLN with 0.01, 0.03, 0.05, 0.15 and 0.30 M $AgNO_3$ solutions at 90°C for 5 h. The mineralogical and textural properties of the raw and Ag-treated CLNs were investigated using X-ray diffraction, X-ray fluorescence and nitrogen gas adsorption analysis. The specific surface area and microporous area values of the Ag-exchanged samples were slightly lower than those of raw CLN. The H_2 adsorption capacities of the Ag-modified forms, measured at 77 K, decreased with increasing $AgNO_3$ molarity after reaching an optimal threshold value of 0.01 M. The H_2 uptake values ranged between 0.317 and 1.056 mmol g^{-1}. The results of the study are explained as depending on the molarity of the $AgNO_3$ solution used for cation exchange.

Keywords: Adsorption; cation exchange; clinoptilolite; hydrogen; XRD

(Received 28 October 2025 UTC; revised 18 February 2026 UTC; accepted 11 June 2026 UTC; Accepted Manuscript published online: 6 July 2026 UTC; Editor: George Christidis)

Porous materials have an internal network of pores of various sizes, ranging from micropores to macropores. These pores significantly increase the materials' specific surface area, making them ideal for use in a wide range of applications across various industrial sectors. Their high porosity and adjustable pore size enable interaction with gases and liquids. This greater porosity increases adsorption capacity and reactivity, making these materials ideal for use in catalytic and energy-related applications, such as catalysis, energy storage and environmental technologies. Hierarchical porous materials, for instance, comprise multiple levels of porosity and demonstrate superior performance in this area due to their greater mass transport and increased active site accessibility, both of which are essential for energy storage and catalysis applications (Yang *et al.*, 2017; Wu *et al.*, 2020).

Currently, the global energy demand is primarily met through the use of fossil fuels, such as coal, oil and natural gas. However, the depletion of these reserves and environmental constraints due to CO_2 emissions have necessitated the development of other sustainable energy sources, such as hydrogen energy. One method of storing hydrogen energy is physical adsorption, in which hydrogen gas is absorbed into the channels and voids of porous materials such as zeolites, metal–organic frameworks (MOFs) and activated carbon. Furthermore, designing materials with specific pore structures enables them to be used in additional applications, including photocatalysis, biomedicine and environmental sensing (Sun *et al.*, 2016).

Zeolites are aluminosilicate minerals (Gottardi & Galli, 1985). The fundamental structural units of zeolites are TO_4 tetrahedra, where T denotes either a silicon or an aluminium atom. The combination of these tetrahedral units forms three-dimensional channel systems and pore networks. These channels contain water molecules, as well as extra-framework exchangeable cations such as Na^+, K^+ and Ca^{2+} (Armbruster & Gunter, 2001). These exchangeable cations balance the negative charge in the zeolite structure resulting from the substitution of silicon atoms by aluminium atoms (Passaglia & Sheppard, 2001). There are more than 40 different types of natural zeolite frameworks, which exhibit a variety of channel structures due to their different arrangements of tetrahedral blocks (Armbruster & Gunter, 2001). One of the most common types of zeolite is clinoptilolite (CLN), which belongs to the heulandite (HEU) group. Its chemical formula is $(Na,K)_6(Al_6Si_{30}O_{72}).20H_2O$. CLN has a monoclinic framework crystal structure with $C2/m$ symmetry and the following unit cell parameters: $a = 17.62$ Å, $b = 17.91$ Å, $c = 7.39$ Å and $\beta = 116°16'$ (Armbruster & Gunter, 2001). Despite sharing the same framework structure, CLN is more thermally stable than HEU (Mumpton, 1960). The two-dimensional channel network of CLN comprises three principal channels: channel A, which has 10 members, and channel B, which has 8 members, run along the c-axis, while channel C, which has 8 members, intersects channels A and B along the a-axis. Consequently, diffusion of molecules along the b-axis is not permitted by the CLN channel system (Gottardi & Galli, 1985; Armbruster & Gunter, 2001). The four extra-framework cation sites (designated M(1), M(2), M(3) and M(4)) have been exten-

Corresponding author: Burcu Erdoğan; Email: burcuerdogan@eskisehir.edu.tr
Cite this article: Erdoğan B and Ergürhan O (2026) Hydrogen adsorption properties of Ag-exchanged clinoptilolite. *Clay Minerals* **61**, 271–276. https://doi.org/10.1180/clm.2026.10052

© The Author(s), 2026. Published by Cambridge University Press on behalf of The Mineralogical Society of the United Kingdom and Ireland.

sively studied within the CLN channel system. The M(1) site in channel A is usually occupied by Na^+ and Ca^{2+}. Additionally, the M(4) site, which is also present within channel A, has a lower occupancy rate than the M(1) site. This site is occupied by Mg^{2+} cations coordinated to water molecules. Ca^{2+} and Na^+ cations have been shown to be located at the M(2) site in channel B. The M(3) site, located in the centre of channel C, is occupied by K^+ cations (Ackley *et al.*, 1992; Jayaraman *et al.*, 2005; Kennedy & Tezel, 2018). In addition to the aforementioned cations, Ag^+ cations can be found in regions M(1) and M(2), as well as in a third region in channel A near the intersection of channels A, B and C (Dimova *et al.*, 2011; Kennedy *et al.*, 2019).

In addition to its catalytic performance (Pérez Vélez *et al.*, 2012; Grzeszczak *et al.*, 2023), CLN can be used as an adsorbent to remove heavy metal ions from wastewater (Inglezakis, 2012; Stepova & Konanets, 2024) and to separate gas mixtures (Grzeszczak *et al.*, 2023; Hedayati *et al.*, 2023; Chen *et al.*, 2024). The catalytic and adsorption properties of CLN can be improved through acid treatment, which positively impacts the specific surface area and number of acid sites (Christidis *et al.*, 2003; Ates & Hardacre, 2012; Karousos *et al.*, 2016; Ghahri *et al.*, 2017). However, this process can result in the rapid collapse of the CLN structure, even at low acid molarities (Garcia-Basabe *et al.*, 2010). Therefore, ion exchange is commonly employed in the literature as an alternative to acid treatment (Rodríguez-Iznaga *et al.*, 2022; Yordanova *et al.*, 2023; Kalvachev *et al.*, 2024; Maia *et al.*, 2024). Ag-exchanged CLNs have been investigated for use in ozone degradation and decomposition (Nikolov *et al.*, 2010; Barbov *et al.*, 2023), as antibacterial materials (De la Rosa-Gómez *et al.*, 2008; Copcia *et al.*, 2011; Znak *et al.*, 2021), as photocatalysts (Hallajiqomi *et al.*, 2019), in dielectric applications (Bunyatova *et al.*, 2016) and in wound dressings (Hubner *et al.*, 2020). However, research on the gas adsorption properties of natural zeolites for hydrogen storage – an alternative energy source that could help meet today's growing energy demands – is limited (Ramesohl & Merten, 2006; Erdoğan Alver & Sakızcı, 2019; Erdoğan & Dikmen, 2020). Furthermore, studies specifically investigating the impact of Ag^+ cation exchange on the hydrogen adsorption properties of CLN are scarce (Erdoğan *et al.*, 2025). The main objective of this study was therefore to determine the textural, structural and hydrogen adsorption properties of Ag-exchanged CLN treated with $AgNO_3$ solutions at various concentrations (0.01–0.30 M).

Experimental

Materials and methods

Natural CLN from Gördes was used in this study, and the particle size selected after grinding and sieving of CLN was less than 63 μm. To remove soluble impurities, 5.0 g aliquots of zeolite samples were kept in 100 mL deionized water at 50°C for 2 h. The samples were filtered and dried overnight at 100°C. A total of 5.0 g of each sample was exchanged with 0.01, 0.03, 0.05, 0.15 and 0.30 M $AgNO_3$ solutions at 90°C for 5 h. All of the Ag^+-exchanged forms were separated, washed several times with deionized water at boiling point and dried at room temperature. The samples were then kept in an oven at 120°C for 20 h. Finally, depending on the molarity of the salt solution used in the cation-exchange process, the cation-exchanged samples of the CLN sample were labelled as follows: 0.01-Ag-CLN, 0.03-Ag-CLN, 0.05-Ag-CLN, 0.15-Ag-CLN and 0.30-Ag-CLN. The cation-exchange process was performed using silver nitrate ($AgNO_3$, ≥99.0%; Sigma-Aldrich, Canada).

Instrumentation

X-ray powder diffraction (XRD) traces of CLN were collected on a Bruker D8 Advance X-ray diffractometer (USA) at room temperature using Cu-*K*α radiation (λ = 1.542 Å) at 40 kV and 40 mA. The scanning step was 0.02° within the range of 5–40°2θ. Elemental analysis of all CLN samples was performed using a Rigaku ZSX Primus instrument. Loss on ignition (LOI) was determined by measuring the mass change after heating to 1000°C at a rate of 10°C min^{-1} and then cooling to room temperature at the same rate. Specific surface areas and micropore data were obtained from N_2 adsorption measurements at 77 K, and hydrogen adsorption isotherms were measured at 77 K up to a pressure of 113 kPa. N_2 and H_2 adsorption analyses of CLN samples were performed using a 3Flex volumetric apparatus (Micromeritics, USA) after degassing at 300°C for 8 h with high-purity (99.999%) nitrogen and hydrogen gases.

Results and discussion

Chemical analysis

The chemical compositions of the main oxides of all of the CLN samples are given in Table 1. Although CLN is rich in calcium and potassium, the chemical composition of the samples changed significantly as the $AgNO_3$ molarity increased. In particular, the MgO, CaO and Na_2O components, rather than the K_2O component, significantly decreased after cation-exchange treatments. This can be attributed to the relatively large size of the K^+ cation compared to the other cations (Na^+, Ca^{2+} and Mg^{2+}) and to its location in the CLN channels. As expected, the Ag_2O composition (wt.%) of the Ag^+-exchanged forms increased with the molarity of the $AgNO_3$ solution.

XRD analysis

The XRD traces of raw CLN and its Ag-exchanged forms are presented in Fig. 1. The CLN sample exhibited characteristic CLN peaks at d = 8.95, 7.91, 3.96 and 2.79 Å, corresponding to 9.88°2θ, 11.17°2θ, 22.50°2θ and 32.01°2θ, respectively (Moore & Reynolds Jr, 1997). Using Esenli and Sirkecioğlu's method (Esenli & Sirkecioğlu, 2005), it was determined that the CLN sample consists mainly of CLN minerals (80–85%), with small amounts of feldspar (3%), opal-A (5–10%) and illite (2%). The illite peak is slightly sharper in the Ag-treated samples than in the raw CLN. Additionally, no change in the intensity of the opal-A peak was observed in the samples. Following cation exchange with Ag^+, however, the intensity of the CLN peaks decreased with increasing solution concentration. The most significant decrease occurred in the 020 reflection at ∼9.88°2θ. The decrease in the intensity of the first two XRD peaks with increasing $AgNO_3$ concentration can be attributed to differences in chemical composition. Similar decreases in the peak intensity of CLN have been observed in previous studies following Ag^+ exchange (Akdeniz & Ülkü, 2008; Dimova *et al.*, 2011; Ünaldi *et al.*, 2013; Kennedy & Tezel, 2018; Erdoğan *et al.*, 2025).

Nitrogen adsorption

The N_2 adsorption isotherms of raw CLN and its cation-exchanged forms at 77 K are shown in Fig. 2. According to the International Union of Pure and Applied Chemistry (IUPAC) classification, all

https://doi.org/10.1180/clm.2026.10052 Published online by Cambridge University Press

Table 1. The chemical composition (wt.%) of raw CLN and its Ag-exchanged forms.

Sample	SiO_2	Al_2O_3	Fe_2O_3	MgO	CaO	Na_2O	K_2O	Ag_2O	LOI
Raw CLN	71.50	11.90	0.98	0.70	2.17	0.79	5.00	–	6.96
0.01-Ag-CLN	71.37	11.67	0.92	0.56	1.87	0.55	4.75	1.31	6.93
0.03-Ag-CLN	71.81	11.71	0.70	0.44	1.67	0.63	4.36	2.50	5.98
0.05-Ag-CLN	70.84	12.02	0.88	0.53	1.37	–	4.15	3.68	6.48
0.15-Ag-CLN	69.46	11.58	0.84	0.36	0.81	0.40	3.80	6.51	6.16
0.30-Ag-CLN	69.90	11.55	0.87	0.30	0.50	–	3.45	7.50	5.84

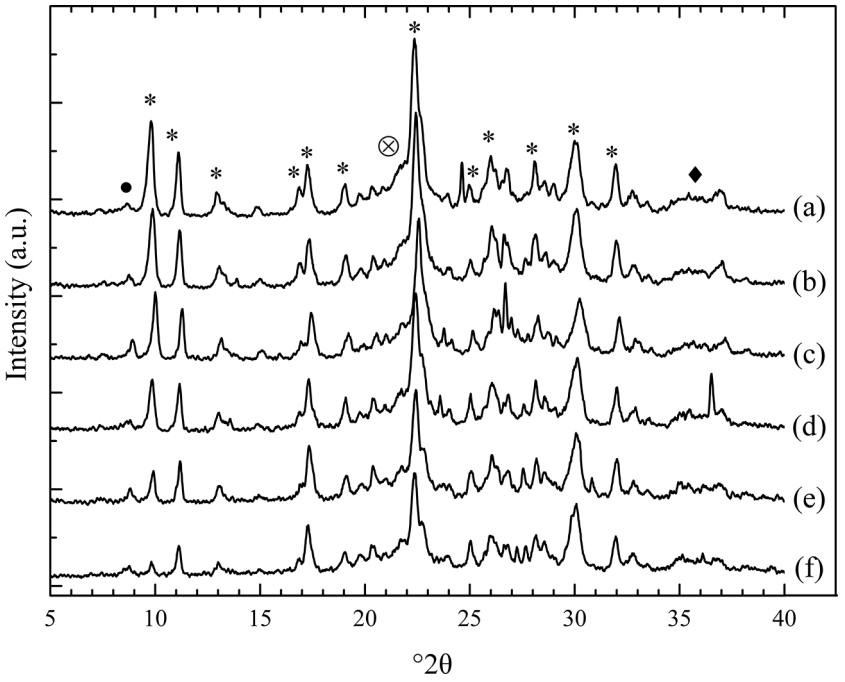


Figure 1. XRD traces of CLN and its Ag^{+}-exchanged forms: (a) CLN, (b) 0.01-Ag-CLN, (c) 0.03-Ag-CLN, (d) 0.05-Ag-CLN, (e) 0.15-Ag-CLN and (f) 0.30-Ag-CLN. * = CLN; • = illite; ⊕ = opal-A; ◆ = feldspar.

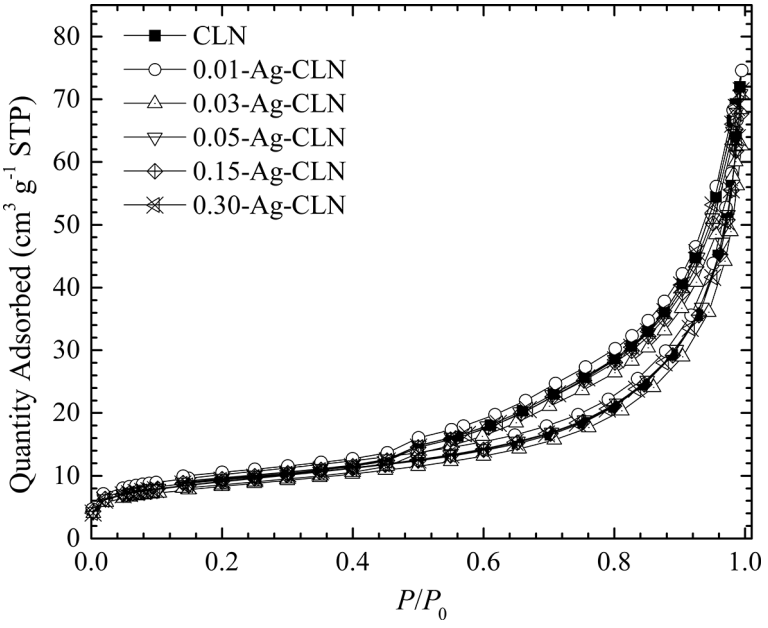


Figure 2. N_2 adsorption–desorption isotherms of CLN and its Ag-exchanged forms at 77 K. STP = standard temperature and pressure.

isotherms display a Type IV character (Sing, 1985), typical of microporous/mesoporous adsorbents. At the adsorption branch, the initial part of the isotherm resembles the Type-II isotherm, involving monolayer–multilayer adsorption. Type-IV isotherms are characterized by a hysteresis loop linked to pore condensation (Lowell *et al.*, 2004). The Brunauer–Emmett–Teller (BET) specific surface area of the raw CLN sample determined by nitrogen adsorption experiments at 77 K was 35.7 $m^2\ g^{-1}$. The specific surface areas of the cation-modified samples exhibited a range of 32.1–36.7 $m^2\ g^{-1}$ (Table 2). The specific surface areas of the Ag-modified CLN samples decreased after exceeding the 0.01 M threshold concentration due to the blockage of the channel

https://doi.org/10.1180/clm.2026.10052 Published online by Cambridge University Press

Table 2. N_2 and H_2 adsorption data for the raw CLN and its Ag-exchanged forms at 77 K.

Sample	BET surface area ($m^2\ g^{-1}$)	Micropore surface area ($m^2\ g^{-1}$)	Micropore volume ($\times 10^{-2}\ cm^3\ g^{-1}$)	H_2 adsorption (mmol g^{-1}/wt.%)
Raw CLN	35.8	9.9	0.42	0.894/0.180
0.01-Ag-CLN	36.7	11.2	0.46	1.056/0.212
0.03-Ag-CLN	29.9	7.1	0.28	0.639/0.129
0.05-Ag-CLN	33.5	8.4	0.37	0.374/0.075
0.15-Ag-CLN	32.6	8.4	0.35	0.320/0.065
0.30-Ag-CLN	32.2	6.6	0.28	0.317/0.064

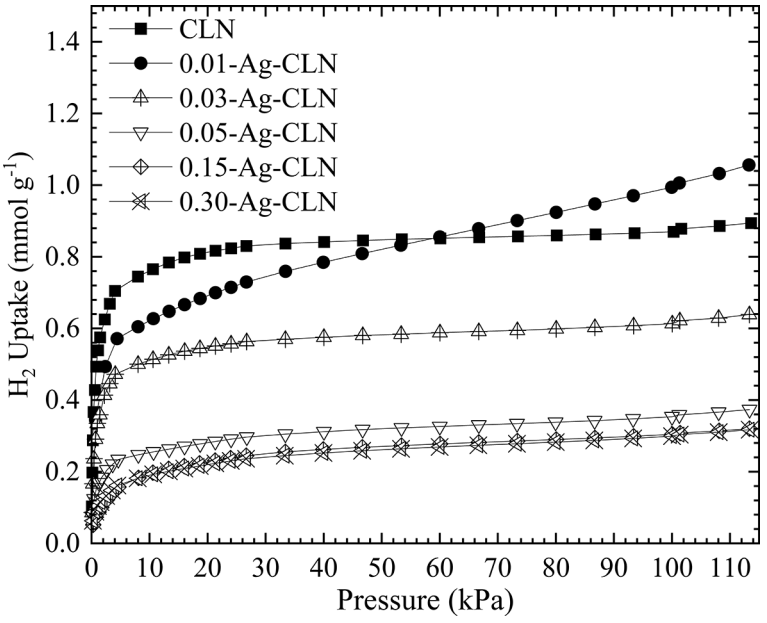


Figure 3. H_2 adsorption isotherms of the CLN and its Ag-exchanged forms at 77 K.

structure of CLN caused by an increase in cation molarity. This results in reduced access of N_2 to the micropore space. Similarly, the 0.01-Ag-CLN sample exhibited the highest micropore area, at 11.2 $m^2\ g^{-1}$. Finally, as with the BET specific surface area, the micropore surface areas of the cation-modified samples also decreased after the 0.01-Ag-CLN sample. Table 2 presents the BET specific surface area and micropore data for all of the samples. The BET specific surface area of all cation-exchanged samples except the 0.01-Ag-CLN sample is smaller than that of the CLN sample. The decrease in BET and microporous surface areas observed in ion-exchanged CLN containing Ag^+ cations is consistent with findings reported in previous studies of CLN (Ünaldi *et al.*, 2013; Kennedy & Tezel, 2018; Erdoğan *et al.*, 2025).

Hydrogen adsorption

The hydrogen adsorption isotherms of raw CLN and its Ag-exchanged forms at 77 K and pressures up to 113 kPa are shown in Fig. 3. The hydrogen retention of the CLN samples decreased in the following order: 0.01-Ag-CLN > CLN > 0.03-Ag-CLN > 0.05-Ag-CLN > 0.15-Ag-CLN > 0.30-Ag-CLN (Table 2). The 0.01-Ag-CLN sample had the highest uptake (0.212 wt.%; 1.056 mmol g^{-1}), while the lowest hydrogen adsorption capacity was exhibited by 0.30-Ag-CLN (0.064 wt.%; 0.317 mmol g^{-1}). Figure 4 shows the specific surface area and H_2 retention of CLN samples against the molarity of $AgNO_3$ solution used in cation-exchange processes. When the 0.01 M threshold was exceeded, both the BET specific surface area and the H_2 adsorption value decreased with increasing molarity of the $AgNO_3$ solution used due to the increasing amount of Ag^+ cations and their position in the structure. However, at the 0.01 M threshold, hydrogen retention improved by ~18% compared to the raw CLN (0.894 mmol g^{-1}). This demonstrates the benefit of applying the cation-exchange process with Ag^+ at low molarity, as this removes most of the other exchangeable cations from the structure, opening the pores and increasing hydrogen adsorption. The hydrogen adsorption capacity of the 0.01-Ag-CLN sample in this study (0.212 wt.%; 1.056 mmol g^{-1}) is higher than that of Cu(I)-[B]-SSZ-13 (0.05 wt.%; Ipek *et al.*, 2018) and of Gördes CLN from the same region exchanged with 1.0 M $NaNO_3$ (0.065 wt.%; Erdoğan Alver & Sakızcı, 2019) and KNO_3 (0.171 wt.%; Erdoğan Alver & Sakızcı, 2019). However, the result obtained for 0.01-Ag-CLN is lower than that of Gördes CLN activated with 2.0 M HNO_3 (0.482 wt.%; Erdoğan & Dikmen, 2020), Gördes CLN treated with 0.5$AgNO_3$ after calcining these samples at 450°C for 6 h (1.181 mmol g^{-1}; Ergürhan & Erdoğan, 2025), Demirci CLN treated with 0.02 M $AgNO_3$ (3.239 mmol g^{-1}; Erdoğan *et al.*, 2025) and NaY (1.19 wt.%; Raj *et al.*, 2012), zeolite-X (1.60 wt.%; Kurniawan *et al.*, 2018) and ZSM-5-O (0.604 wt.%; Fujiwara *et al.*, 2014) due to the textural and structural differences. The lower H_2 uptake obtained in this study for 0.01-Ag-CLN compared to H_2 uptake obtained for Demirci CLN treated with 0.02 M $AgNO_3$ can be attributed to differences in particle size between the Gördes and Demirci samples, differences in the Si/Al ratio, differences in pre-degassing temperature prior to hydrogen adsorption experiments and differences in process temperature and duration for ion exchange with $AgNO_3$ (Table 3). Although natural CLN has a lower hydrogen adsorption capacity than more expensive synthetic zeolites, it is abundant in nature. Its gas adsorption properties

https://doi.org/10.1180/clm.2026.10052 Published online by Cambridge University Press

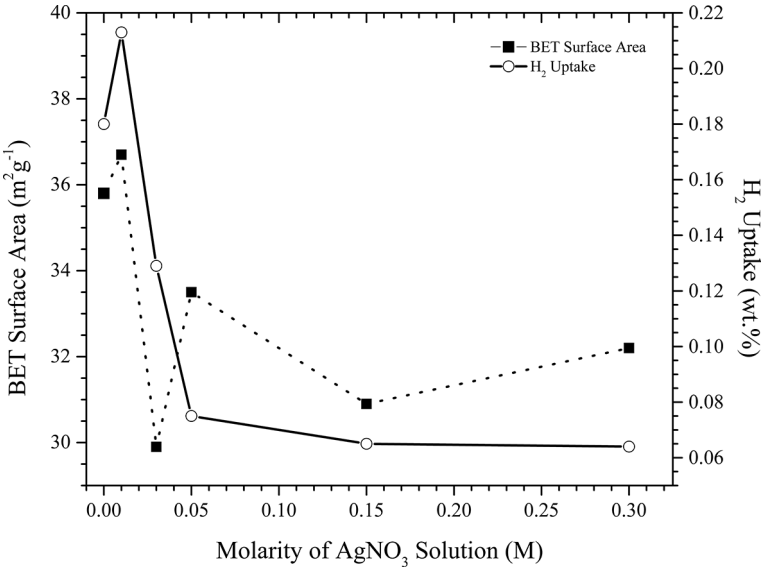


Figure 4. BET specific surface area and H_2 retention of CLN samples *vs* molarity of $AgNO_3$ solution used in the cation-exchange processes.

Table 3. A comparison of the structural, textural and gas adsorption properties of raw and Ag^+-exchanged Gördes and Demirci CLN.

Sample	Particle size (μm)	Si/Al ratio	Ag^+ exchange conditions	Degas conditions	BET/micropore Surface area (m^2 g^{-1})	H_2 adsorption (mmol g^{-1})
Raw-CLN (Gördes)	63	5.09	–	300°C, 8 h	35.8/9.9	0.894
0.01-Ag-G-CLN	63	5.19	0.01 M, 90°C, 5 h	300°C, 8 h	36.7/11.2	1.056
D-CLN (Demirci)[a]	5–10	4.79	–	350°C, 8 h	29.5/15.4	2.714
0.02-Ag-D-CLN[a]	5–10	4.79	0.02 M, 80°C, 4 h	350°C, 8 h	27.5/12.1	3.239

[a]Erdoğan *et al.* (2025).

can be significantly enhanced through modification, providing advantages for hydrogen storage applications. Consequently, the 0.01-Ag-CLN sample, which showed the highest level of hydrogen retention of all of the samples in this study, can be recommended for use in hydrogen storage applications.

Conclusions

In this study, the effects of cation exchange with $AgNO_3$ solution at various molarities (0.01, 0.03, 0.05, 0.15 and 0.30 M) on the physicochemical and hydrogen adsorption properties of CLN were investigated. Increasing the molarity of the exchange solution to obtain various Ag^+-modified forms caused significant changes, particularly in the 020 peak of the CLN sample, due to changes in its chemical composition. The BET specific surface area values of the Ag-exchanged CLN samples (29.9–36.7 m^2 g^{-1}) were similar to that of the original CLN (35.80 m^2 g^{-1}). Significant changes in hydrogen adsorption and BET specific surface areas were observed in the modified CLNs due to the increased molarity of the $AgNO_3$ solution. The 0.01-Ag-CLN sample in this study is a promising candidate for hydrogen storage applications due to its optimal BET specific surface area and hydrogen adsorption capacity. In future studies, it may be advisable to include isothermal adsorption heat measurements at multiple temperatures to provide a mechanical perspective on H_2–surface interactions and to validate the proposed pore-opening mechanism.

Acknowledgements. The authors would like to thank the Ceramic Research Centre (SAM, Eskişehir, Türkiye) for carrying out the XRF analysis of all of the samples.

Financial support. Financial support is gratefully acknowledged from the Scientific Research Committee of Eskisehir Technical University, under grant number 23ADP046.

Competing interests. The authors declare none.

References

Ackley M.W., Giese R.F. & Yang R.T. (1992) Clinoptilolite: untapped potential for kinetics gas separations. *Zeolites*, **12**, 780–788.

Akdeniz Y. & Ülkü S. (2008) Thermal stability of Ag-exchanged clinoptilolite rich mineral. *Journal of Thermal Analysis and Calorimetry*, **94**, 703–710.

Armbruster T. & Gunter M.E. (2001) Crystal structures of natural zeolites. *Reviews in Mineralogy and Geochemistry*, **45**, 1–67.

Ates A. & Hardacre C. (2012) The effect of various treatment conditions on natural zeolites: ion exchange, acidic, thermal and steam treatments. *Journal of Colloid and Interface Science*, **372**, 130–140.

Barbov B., Zaharieva K., Karakashkova P. & Penchev H. (2023) Silver-impregnated zeolitized tuffs for environmental degradation of ozone. *Review of the Bulgarian Geological Society*, **84**, 15–18.

Bunyatova U., Ozturk Koc S., Orbukh V.I., Eyvazova G.M., Agamaliev Z.A., Lebedeva N.N. *et al.* (2016) Peculiarities of the dielectric response of the silver-modified-zeolite porous microstructure. *Superlattices and Microstructures*, **98**, 295–305.

Chen X., Zhou J., Wei J., Cui X., Wan C., Liu M. *et al.* (2024) Performance evaluation of bimetallic ion exchanged clinoptilolite for potential equilibrium and kinetic adsorption separations of CO_2 from CO_2/CH_4 mixture. *Separation and Purification Technology*, **331**, 125563.

Christidis G.E., Moraetis D., Keheyan E., Akhalbedashvili L., Kekelidze N., Gevorkyan R. *et al.* (2003) Chemical and thermal modification of natural HEU-type zeolitic materials from Armenia, Georgia and Greece. *Applied Clay Science*, **24**, 79–91.

https://doi.org/10.1180/clm.2026.10052 Published online by Cambridge University Press

Copcia V.E., Luchian C., Dunca S., Bilba N. & Hristodor C.M. (2011) Antibacterial activity of silver-modified natural clinoptilolite. *Journal of Materials Science*, **46**, 7121–7128.

De la Rosa-Gómez I., Olguín M.T. & Alcántara D. (2008) Antibacterial behavior of silver-modified clinoptilolite–heulandite rich tuff on coliform microorganisms from wastewater in a column system. *Journal of Environmental Management*, **88**, 853–863.

Dimova L., Petrov O., Kadiyski M., Lihareva N., Stoyanova-Ivanova A. & Mikli V. (2011) Preparation and Rietveld refinement of Ag-exchanged clinoptilolite. *Clay Minerals*, **46**, 205–212.

Erdoğan B. & Dikmen G. (2020) Effect of the acid type on clinoptilolite-rich tuff for hydrogen storage. *International Journal of Hydrogen Energy*, **45**, 2017–2021.

Erdoğan B., Ekinci Şans B. & Esenli F. (2025) A comparative study on the physicochemical and hydrogen adsorption properties of Ag-exchanged Demirci (Türkiye) clinoptilolites. *International Journal of Hydrogen Energy*, **145**, 1144–1151.

Erdoğan Alver B. & Sakızcı M. (2019) Hydrogen (H_2) adsorption on natural and cation-exchanged clinoptilolite, mordenite and chabazite. *International Journal of Hydrogen Energy*, **44**, 6748–6755.

Ergürhan O. & Erdoğan B. (2025) Effect of NH_4NO_3 pre-treatment on hydrogen adsorption properties of Na^+, K^+ Ag^+, Li^+ H^+, Ni^{2+} Ca^{2+}, Cu^{2+} and Mg^{2+} exchanged natural clinoptilolite. *International Journal of Hydrogen Energy*, **144**, 200–210.

Esenli F. & Sirkecioğlu A. (2005) The relationship between zeolite (heulandite–clinoptilolite) content and the ammonium-exchange capacity of pyroclastic rocks in Gördes, Turkey. *Clay Minerals*, **40**, 557–564.

Fujiwara M., Fujio Y., Sakurai H., Senoh H. & Kiyobayashi T. (2014) Storage of molecular hydrogen into ZSM-5 zeolite in the ambient atmosphere by the sealing of the micropore outlet. *Chemical Engineering and Processing: Process Intensification*, **79**, 1–6.

Garcia-Basabe Y., Rodriguez-Iznaga I., de Menorval L.-C., Llewellyn P., Maurin G., Lewis D.W. *et al.* (2010) Step-wise dealumination of natural clinoptilolite: structural and physicochemical characterization. *Microporous and Mesoporous Materials*, **135**, 187–196.

Ghahri A., Golbabaei F., Vafajoo L., Mireskandari S.M., Yaseri M. & Shahtaheri S.J. (2017) Removal of greenhouse gas (N_2O) by catalytic decomposition on natural clinoptilolite zeolites impregnated with cobalt. *International Journal of Environmental Research*, **11**, 327–337.

Gottardi G. & Galli E. (1985) *Natural Zeolites*. Springer Berlin Heidelberg, Berlin, Germany, 409 pp.

Grzeszczak J., Wróblewska A., Kiełbasa K., Koren Z.C. & Michalkiewicz B. (2023) The application of clinoptilolite as the green catalyst in the solvent-free oxidation of α-pinene with oxygen. *Sustainability*, **15**, 10381.

Hallajiqomi M., Mehdipourghazi M. & Varaminian F. (2019) Degradation of tetracycline using photocatalytic membrane reactor with nanocomposite Ag doped clinoptilolite zeolite photocatalyst. *Desalination and Water Treatment*, **139**, 111–122.

Hedayati A., Delica B.A., Perez-Gil S. & Prieto-Fernandez S. (2023) Evaluation of high-performance adsorbents for separation of CO_2 from industrial effluent gases. *Greenhouse Gases: Science and Technology*, **13**, 216–226.

Hubner P., Donati N., Quines L.K.d.M., Tessaro I.C. & Marcilio N.R. (2020) Gelatin-based films containing clinoptilolite-Ag for application as wound dressing. *Materials Science and Engineering: C*, **107**, 110215.

Inglezakis V.J. (2012) Modified zeolites: pretreatment of natural zeolites by use of inorganic salts. Pp. 156–165. in: *Handbook of Natural Zeolites* (V.J. Inglezakis & A.A. Zorpas, editors). Bentham Science Publishers, Sharjah, United Arab Emirates.

Ipek B., Pollock R.A., Brown C.M., Uner D. & Lobo R.F. (2018) H_2 adsorption on Cu(I)–SSZ-13. *The Journal of Physical Chemistry C*, **122**, 540–548.

Jayaraman A., Yang R.T., Chinn D. & Munson C.L. (2005) Tailored clinoptilolites for nitrogen/methane separation. *Industrial & Engineering Chemistry Research*, **44**, 5184–5192.

Kalvachev Y., Vitale E., Arena C., Todorova T., Ilkov D. & Velikova V. (2024) Ion-exchanged clinoptilolite as a substrate for space farming. *Agriculture*, **14**, 350.

Karousos D.S., Sapalidis A.A., Kouvelos E.P., Romanos G.E. & Kanellopoulos N.K. (2016) A study on natural clinoptilolite for CO_2/N_2 gas separation. *Separation Science and Technology*, **51**, 83–95.

Kennedy D.A. & Tezel F.H. (2018) Cation exchange modification of clinoptilolite – screening analysis for potential equilibrium and kinetic adsorption separations involving methane, nitrogen, and carbon dioxide. *Microporous and Mesoporous Materials*, **262**, 235–250.

Kennedy D.A., Khanafer M. & Tezel F.H. (2019) The effect of Ag^+ cations on the micropore properties of clinoptilolite and related adsorption separation of CH_4 and N_2 gases. *Microporous and Mesoporous Materials*, **281**, 123–133.

Kurniawan R.Y., Romadiansyah T.Q., Tsamarah A.D. & Widiastuti N. (2018) Synthesis of zeolite-X from bottom ash for H_2 adsorption. P. 012083. in: *IOP Conference Series: Materials Science and Engineering*. IOP Publishing, Bristol, UK.

Lowell S., Shields J.E., Thomas M.A. & Thommes M. (2004) *Characterization of Porous Solids and Powders: Surface Area, Pore Size and Density*. Springer Netherlands, Dordrecht, The Netherlands, 349 pp.

Maia D.A.S., Azevedo T.M., Pereira D.S., Castro R.A.M., Nascimento B.O., Rodríguez-Castellón E. *et al.* (2024) Water vapor adsorption on small pore ion-exchanged zeolites. *Adsorption*, **30**, 507–517.

Moore D.M. & Reynolds Jr R.C. (1997) *X-Ray Diffraction and the Identification and Analysis of Clay Minerals*, 2nd edition. Oxford University Press, New York, NY, USA, 400 pp.

Mumpton F.A. (1960) Clinoptilolite redefined. *American Mineralogist*, **45**, 351–369.

Nikolov P., Genov K., Konova P., Milenova K., Batakliev T., Georgiev V. *et al.* (2010) Ozone decomposition on Ag/SiO_2 and Ag/clinoptilolite catalysts at ambient temperature. *Journal of Hazardous Materials*, **184**, 16–19.

Passaglia E. & Sheppard R.A. (2001) The crystal chemistry of zeolites. *Reviews in Mineralogy and Geochemistry*, **45**, 69–116.

Pérez Vélez R., Elizalde González M.P. & Bentrup U. (2012) Preparation and *in situ* spectroscopic characterization of Cu-clinoptilolite catalysts for the oxidative carbonylation of methanol. *Microporous and Mesoporous Materials*, **164**, 93–98.

Raj M.C., Prasanth K.P., Dangi G.P. & Bajaj H.C. (2012) Hydrogen sorption in transition metal exchanged zeolite Y: volumetric measurements and simulation study. *Journal of Porous Materials*, **19**, 657–666.

Ramesohl S. & Merten F. (2006) Energy system aspects of hydrogen as an alternative fuel in transport. *Energy Policy*, **34**, 1251–1259.

Rodríguez-Iznaga I., Shelyapina M.G. & Petranovskii V. (2022) Ion exchange in natural clinoptilolite: aspects related to its structure and applications. *Minerals*, **12**, 1628.

Sing K.S.W. (1985) Reporting physisorption data for gas/solid systems with special reference to the determination of surface area and porosity (Recommendations 1984). *Pure and Applied Chemistry*, **57**, 603–619.

Stepova K. & Konanets R. (2024) Clinoptilolite- and glauconite-based sorbents for lead removal from natural waters. *Journal of Environmental Engineering and Landscape Management*, **32**, 191–200.

Sun M.-H., Huang S.Z., Chen L.H., Li Y., Yang X.Y., Yuan Z.Y. & Su B.L. (2016) Applications of hierarchically structured porous materials from energy storage and conversion, catalysis, photocatalysis, adsorption, separation, and sensing to biomedicine. *Chemical Society Reviews*, **45**, 3479–3563.

Ünaldi T., Mizrak I. & Kadir S. (2013) Physicochemical characterisation of natural K-clinoptilolite and heavy-metal forms from Gördes (Manisa, western Turkey). *Journal of Molecular Structure*, **1054**, 349–358.

Wu L., Li Y., Fu Z. & Su B.L. (2020) Hierarchically structured porous materials: synthesis strategies and applications in energy storage. *National Science Review*, **7**, 1667–1701.

Yang X.Y., Chen L.H., Li Y., Rooke J.C., Sanchez C. & Su B.L. (2017) Hierarchically porous materials: synthesis strategies and structure design. *Chemical Society Reviews*, **46**, 481–558.

Yordanova I., Hristov S., Kolev H., Todorova S. & Naydenov A. (2023) Cobalt–manganese ion-exchanged clinoptilolite supported catalysts for *n*-hexane oxidation. *Catalysis Today*, **423**, 114267.

Znak Z.O., Kornii S.A., Mashtaler A.S. & Zin O.I. (2021) Production of nanoporous zeolites modified by silver ions with antibacterial properties. *Materials Science*, **56**, 536–543.

https://doi.org/10.1180/clm.2026.10052 Published online by Cambridge University Press